Influence of Stress State Conditions on Densification Behavior of Titanium Sponge

Ivan Berezin[1,2], Anton Nesterenko[1], Alexandr Zalazinskii[1], George Kovacs[3]

[1] Institute of Engineering Science, Ural Branch, Russian Academy of Sciences
Komsomolskaya Str. 34, 620049 Ekaterinburg, Russia
berezin@imach.uran.ru, nav@imach.uran.ru, agz@imach.uran.ru
[2] Ural Federal University, Mira Str. 19, 620002 Ekaterinburg, Russia
i.m.berezin@urfu.ru
[3] Computer and Automation Institute, Hungarian Academy of Sciences,
Kende u. 13-17, H-1111 Budapest, Hungary, györgy.kovacs@sztaki.hu

Abstract: The paper discusses the material compaction process under various types of stress conditions based on the simulation of the multiaxial compression process of powdered titanium sponge. The finite element model of the multiaxial compression process made it possible to apply both radial and axial pressure independently from one another. Titanium sponge subjected to reversible thermo-hydrogen processing was used as the research material. For the description of the material plasticity condition, the modified Drucker–Prager Cap plasticity model was used, implemented in Abaqus.

Keywords: stress state; multiaxial compression; titanium sponge; metal powder; modified Drucker–Prager Cap plasticity model; representative unit cell; micromechanical model; finite element simulation

1 Introduction

The intensification of the compaction mechanism of metal powders heavily depends on the choice of an effective deformation scheme, providing the reduction of the compaction forces, at the increase in the density of the compacted work-piece. It is known [1–4] that achieving high densities of a deformable porous solid is only possible in the processes that implement optimal combinations of normal and tangential pressures.

In this connection, one should expect that the problem of the increasing density in a work-piece may be solved based on a complex analysis of stressed state effect on compaction and improvement of existing load distribution schemes. At that, the correlation between the compacting pressure and the material density mostly

relates to those deformation schemes, for which it was obtained. Thus, finding a consistent pattern of changing the material density depending on the value of shear and normal stresses at various deformation schemes is a relevant objective.

The most complete research of the regular pattern of material compaction may be based on the use of triaxal (multiaxial) compression processes [5–7]. This type of experimental equipment must provide different stress conditions in a work-piece by a possibility to apply both radial and axial pressure independently. The complexity of experiments and low effectiveness of triaxial compression installations make this approach expensive and inefficient.

The widespread industrial technology for the production of titanium blanks and articles includes the manufacture of titanium sponge, which is a high-purity noncompact titanium. Further processing of spongy titanium is characterized by large losses of metal in the form of recurrent and irretrievable losses. In addition, the technology of production of titanium blanks and other products is a multistage one, and is characterized by high energy and labor costs. For example, according to an assessment [8] in the cost of a 25 mm titanium sheet the sponge represets only 25 per cent.

Powder metallurgy methods and additive technologies allow to radically increase the utilization of metal raw materials and to reduce production costs. At the same time, the titanium sponge and powder compositions can be the commercially most available base material for such technologies. Manufactured products can be used in medicine, transport engineering, production of consumer goods, architecture, in desalination plants, and it also may be used as pipeline fittings in chemistry, petrochemistry, food industry, etc.

The possibility of manufacturing titanium products with the required properties, obtained by solid-phase consolidation technology of a titanium sponge, is shown in numerous studies [9–16]. The favorable effect of preliminary thermohydrogen treatment for the compactibility of a titanium sponge at certain temperatures has been first studied and shown in [17, 18].

In the present work a finite element (FE) simulation of the process of multiaxial compression of powdered titanium sponge is carried out. The purpose is the identification of material compaction quantitative pattern, where the pattern depends on the combination of equivalent pressure stress and von Mises equivalent stresses.

2   Unit Cell and Yield Criterion

The powdered titanium sponge subjected to reversible thermo-hydrogen treatment was used as material for the study (Figure 1). The hydrogenating was carried out by way of thermal diffusion in a Sieverts type vacuum machine. Titanium

saturation up to the concentration of 0.5 wt% of hydrogen at the compaction process temperature of 325 °C makes it possible to seriously reduce the compaction forces [17]. At that, the hydrogen alloying is temporary, and after the operation of plastic deformation, the hydrogen is removed by vacuum annealing.
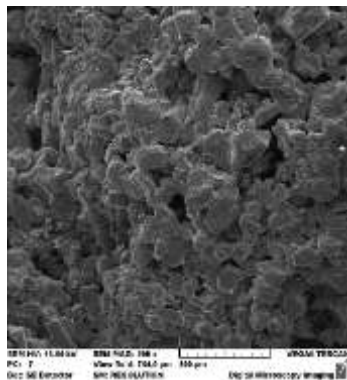

Figure 1
Fragment of titanium sponge structure

The process of material compaction was studied at two scale levels.

At the macrolevel scale, the powdered titanium sponge is entirely homogenous, isotropic, plastically compressible continuum solid. The Drucker–Prager Cap plasticity model (MDPC) has been applied for the description of the titanium sponge yield criterion [19].

$$f_1 = q - d - p \tan \beta = 0 \,,$$

$$f_2 = \sqrt{(p-c)^2 + \left(\frac{R}{1+\alpha - \alpha/\cos\beta} q \right)^2} - m = 0 \,, \tag{1}$$

$$f_3 = \sqrt{(p-c)^2 + \left[q - \left(1 - \frac{\alpha}{\cos\beta}\right)\frac{n}{\alpha} \right]^2} - n = 0$$

where q – von Mises equivalent stresses, p – mean normal pressure, d – cohesion of the material, β – angle of friction of the material, R – parameter that controls the shape of the cap, α – coefficient used to define a transition yield surface f_2 (assumed to be equal to 0.05). The functions of the material condition c, m and n may be presented as:

$$c = \frac{p_b - Rd}{1 + R \cdot \tan\beta} \,,$$

$$m = R(d + c \cdot \tan\beta), \tag{2}$$

$$n = \alpha\left(d + c \cdot \tan\beta\right)$$

where p_b is the hydrostatic compression yield stress.

The identification of the parameters of the assumed plasticity model involves a series of experiments [20–23]. The methodological complexity of their implementation leads to the attempts of finding more simple ways of plasticity curve identification. In particular, the MDPC yield curve may be approximated with a function having less internal variables, and this approach may be used for the identification of the initial model parameters. For approximation of the initial yield curve, the following equation has been used:

$$q = \gamma\left[\sqrt{2\left(p^*\right)^2 + 1/4} - \left(p^*\right)^2 - 1/2\right]^{1/2} \tag{3}$$

where p^* – mean normal pressure, presented in dimensionless form ($p^* = p/p_b$); γ – the coefficient, bringing the equation (3) into proximity with the modified Drucker–Prager cap yield curve.

Figure 2 shows a qualitative comparison of the geometric interpretation of the (MDPC) plasticity model and the curve built in accordance with the equation (3) in the q–p plane. It is clear that the curves intersect the following points:

A – isostatic decompression yield stress;

B, – lying on the crossing of the straight-line portion of the MDPC curve and the curve in accordance with the equation (3);

C – evolution limit that represents the volumetric inelastic strain driven hardening/softening;

D – isostatic compression yield stress.

Using an additional curve for the identification of the MDPC plasticity model allows only two experiments: die compaction and isostatic compression. At that, it is assumed that the initial particle cohesion is rather small and the yield strength in isostatic decompression is assumed to be closed to zero. Therefore, the material is loose. It is worth mentioning that this work considers only the compaction process; consequently, the stress condition in the deformed material will correspond to the points lying inside the elliptical portion, where the curve set by equation (3) and the Drucker–Prager curve (1) are close to one another. This makes it possible to conclude that an approximating curve may be used as a technique for determining the MDPC model coefficients.
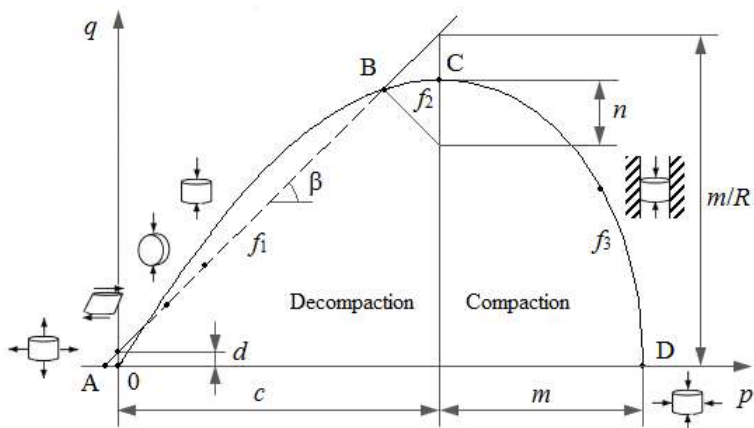
Figure 2

Qualitative comparison of the geometric interpretation of the modified Drucker–Prager cap plasticity model (dashed line) and the approximating curve in accordance with equation (3) (solid line)

Along with the reduction of the number of necessary points for the formig of the plasticity curve, there is a possibility to change the labor consuming natural experiments for the methods based on the theory of micromechanical deformation (microlevel scale) of a representative unit cell [24–26]. The works [27–32] are devoted to choosing a form, particle packing schemes, and to study their interaction and deformation. The results showed a well-founded choice of a cubic array of identical spheres for the definition of metal powder micromechanical model.

In this study, the unit cell is supposed to consist of a single spherical particle with a central pore circumscribed by a cube (Figure 3). The arrangement of a powder has been chosen based on the bulk density of titanium sponge in the initial state.
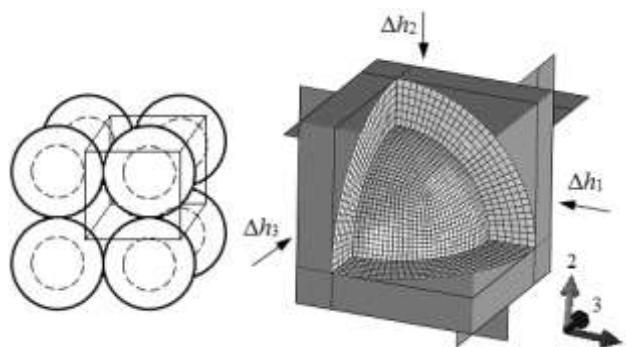

Figure 3a and Figure 3b

Arrangement of powder (3a) and FE model of 1/8 of unit cell (3b)

It is assumed that the considered material has a regular structure and there are no effects related to pulsatory oscillation, rotation and translational motion of the particles. It is important to establish plastic yield stress, shape and void volume changes for the introduced material model. Due to the statistical uniformity of properties, it is sufficient to solve the task only for one representative unit cell. It should be noted that in this work, the material porosity formed by the spherical particle packing, shown in Figure 3a, is understood only as void volume between the particles.

The FE solver Abaqus/Standard was used. The boundary conditions of the particle are the following: nodes at 1–3 plane have U2=UR1=UR3=0 prescribed, nodes at 1–2 plane have U3=UR1=UR2=0 prescribed, nodes at 2–3 plane have U1=UR2=UR3=0 prescribed. The curved surfaces of the particle are traction free. The representative unit cell was deformed by the displacement of boundary condition (Δh_i) fully rigid surfaces, imitating the influence of neighbor particles around the cell. For the isostatic (hydrostatic) compression, $\Delta h_1 = \Delta h_2 = \Delta h_3$ and for the case of die compaction, $\Delta h2 = \Delta h3 = 0$. The particle diameter $d_p = 2$ mm. The choice of particle size for numerical simulation is justified by the position of the statistical mechanics of structurally inhomogeneous materials, according to which the ratio $d_c/d_p \geq 10$, where d_c – container diameter, d_p – particle diameter, must be implemented. For the experimental study, the titanium sponge was screened with an average particle size of 2 mm.The relative density of material at the chosen particle packing diagram is $\rho_{rel} = 0.52$. The Young's modulus $E = 112$ GPa, the Poisson's ratio $\nu = 0.34$. The contact between the particle and the rigid surfaces is modeled with a contact pair. The rigid surfaces are modeled as analytical rigid surfaces. The mechanical interaction between the contact surfaces is assumed to be frictionless. The titanium strain-hardening curve has been taken from [33].

Figure 4 shows the distribution of von Mises equivalent stresses in a particle of the representative unit cell at isostatic compression (Figure 4a) and die compaction (Figure 4b) for porosity $\theta = 17.5\%$.
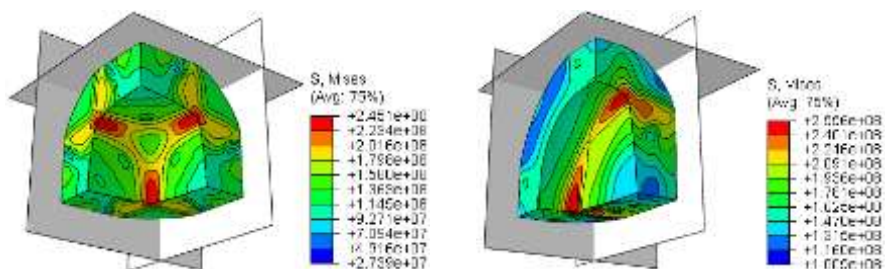

Figure 4a   Figure 4b

Distribution of von Mises equivalent stresses in a particle of the representative unit cell at isostatic compression (4a) and die compaction (4b)

In the case of plastic deformation of particles, the material flows into free space (pores) between them and the point contacts under the load develop into contact surfaces. The volumetric plastic deformation (ε_v^{pl}) was established in accordance with the equation

$$\varepsilon_v^{pl} = \ln(V_0/V), \tag{4}$$

where $V_0 = 1$ – representative unit cell initial volume, V – its volume after deformation.

Based on the obtained values of the components of the stress tensor σ_1, σ_2, σ_3 acting on the unit cell contact areas, the values of von Mises equivalent stress (q) and equivalent pressure stress (p) were determined for two cases of stress condition of the representative unit cell.
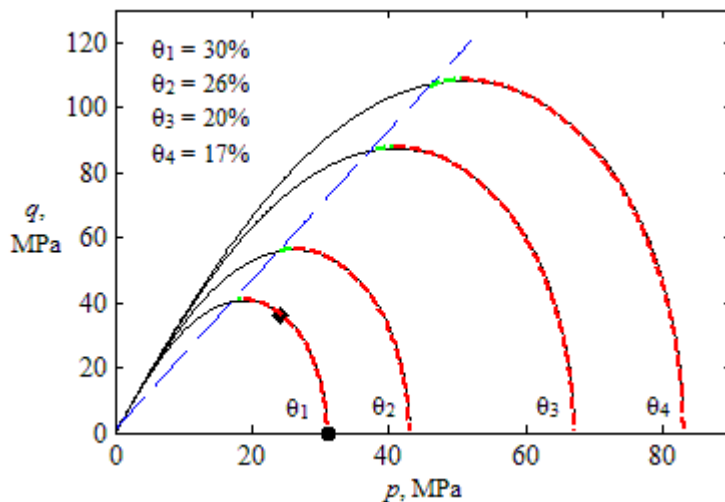

Figure 5
Evolution of the modified Drucker–Prager cap plasticity curve in the p–q plane

In Figure 5, the sign "●" corresponds to the stress condition of isostatic compression, and the sign "♦" – to the stress condition of die compaction. The approximating curve built along the defined points (the solid line in Figure 5) allowed the identification of coefficients of the MDPC model for titanium sponge: $\beta = 66.5°$; $R = 0.276$; $\varepsilon_v^{pl}|_0 = 0$; $\alpha = 0.05$; $d = 1$ MPa.

It should be noted that the hardening of material will inevitably cause changes in the determined coefficients. Nevertheless, the present work uses a default setting of the MDPC plasticity model implemented in Abaqus. Consequently, the coefficients found for specific porosity (θ) will be valid at any level of compaction.

3   Multiaxial Compression Simulation

Figure 6 shows the scheme of the multiaxial compression process.
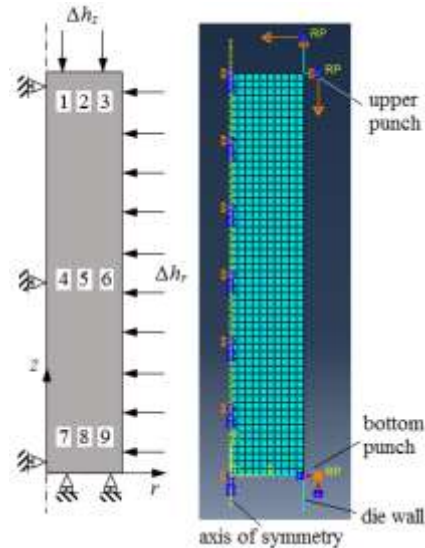

Figure 6
Computational scheme and FE model

The FE model is axisymmetric and includes the half of the billet. In Abaqus/Standard elements of type CAX4R, a 4-node bilinear axisymmetric quadrilateral with reduced integration are used. All parts of the die are fully rigid. The kinematic boundary conditions are symmetric on the axis (nodes at $r = 0$ have $u_r = 0$ prescribed).

The work-piece deformation takes place under hard stress conditions: the upper punch and die wall are displaced by Δh_i using a displacement boundary condition. The bottom punch is fully constrained. The radial pressure is produced on the billet due to the displacement of the matrix wall Δh_r in the radial direction. The height of the billet in initial state $H = 56$ mm, the radius $R = 10$ mm. The given initial porosity of titanium sponge $\theta = 48\%$. The indicated initial porosity of the material has been chosen based on the experimentally established bulk density of the powder used with an average particle size of a titanium sponge ≈ 2 mm. The properties of material are taken at the temperature of 325 °C.

At the first stage, the work-piece was subjected to non-uniform multiaxial compression. The displacement values Δh_z and Δh_r were changed randomly, independently from one another, which made it possible to provide various schemes of the stress state condition.

Moreover, it assists to identify the corresponding values of volumetric plastic deformation (ε_v^{pl}), von Mises equivalent stresses (q) and equivalent pressure stress (p) in areas No. 1-9.

Compression for each scheme of stress state condition continued until porosity (θ) close to zero was achieved in one of the billet areas. In connection with the fact that Abaqus/Standard solver, applied for the FE analysis, by default does not calculate the porosity (θ), the following equation was used:

$$\theta = (1 - \rho_{rel} \cdot \exp(|\varepsilon_v^{pl}|)) \times 100\%. \tag{5}$$

At the second stage of the research, the sample was only subjected to axial compression by way of moving the upper punch to Δh_z value with a fixed position of the matrix wall ($\Delta h_r = \text{const} = 0$). The deformation was stopped upon achievement of quasimonolythic state in one of the work-piece portions. The material porosity was computed according to the equation (5). The corresponding q and p values in areas No. 1–9 on various stages of deformation were determined with the help of the embedded post-processor Abaqus/Viewer. The third stage of experiments included the radial compression of the billet without the punch axial movement ($\Delta h_z = \text{const} = 0$). The values of q, p and ε_v^{pl} were determined in the same way as during the experiments of the first and the second stage. A more detailed description of the modeling of the multiaxial compression simulation is given in the paper [18].

4   Model Verifiation and Discussion

As a result of the FE simulation, the following regression equation was obtained

$$\theta = b_1 \cdot \exp(-b_2 \cdot k_q) + b_3 \cdot \exp(-b_4 \cdot k_p). \tag{6}$$

Here $k_q = q/q_s$, $k_p = p/q_s$, where q_s is the yield stress of material in a nonporous condition. The coefficients in equation (6) have the following meaning: $b_1 = 6.222$, $b_2 = 1.585$, $b_3 = 43.21$, $b_4 = 1.142$. The graphical interpretation of equation (6) is given in Figure 7.

It is clear that the value change of equivalent pressure stress, expressed by the coefficient k_p, produces a more substantial effect on the compaction of material as compared with shear deformation. Nevertheless, the absence of shear deformations in case of a stress condition of uniform isostatic compression ($k_q = 0$) does not allow achieving less than 6% porosity. On the other hand, only shear stresses ($k_p = 0$) do not lead to any substantial reduction of material porosity, whereas the change of θ is not more than 8%. Consequently, production of a quasimonolithic material with a minimal porosity is only possible at the synchronizing action of hydrostatical and shear deformations. When the $k_q = 2$ and $k_p = 4$ are achieved, the porosity is close to zero and any further increase of the coefficient values does not lead to any noticeable compaction of the material.

In order to verify the regression equation (6) obtained by the FE simulation, an experimental research of die compaction of titanium sponge was carried out.

The work-pieces were produced at the pressure of 1000 MPa on upper punch and the temperature of 325 °C. For the determination of porosity, the thin plates in various axial section of work-pieces were produced.
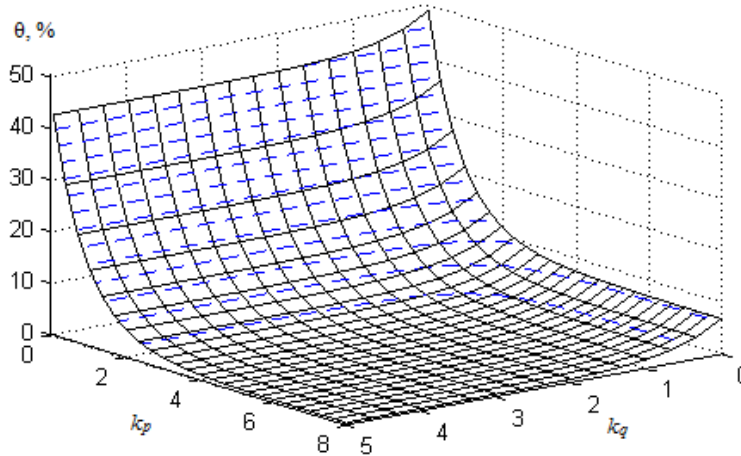

Figure 7
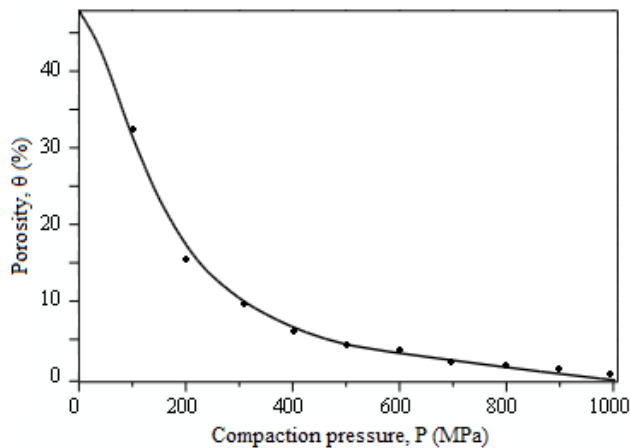Dependency of porosity on the k_q and k_p

Figure 8
Effect of compaction pressure on the average porosity of green workpiece

Figure 8 shows the titanium sponge compaction diagram, depending on the compaction pressure.

The curve in the form of a solid line has been obtained by computer simulation of the compaction process in a closed mold. The dots denote the results of an experimental measurement of the average volumetric porosity of briquettes in the compacting pressure range from 100 to 1,000 MPa. It can be seen that at compaction pressure of up to 400 MPa the compaction process is quite intensive and the average bulk porosity of the briquette varies from 48% to 7%. Further, the compaction intensity decreases, in the pressure range from 400 to 1,000 MPa, the average volumetric porosity decreases from 7% to 1-2%. The mechanism of compaction of a titanium sponge is similar to the behavior of a metal powder subjected to compaction in a closed mold.
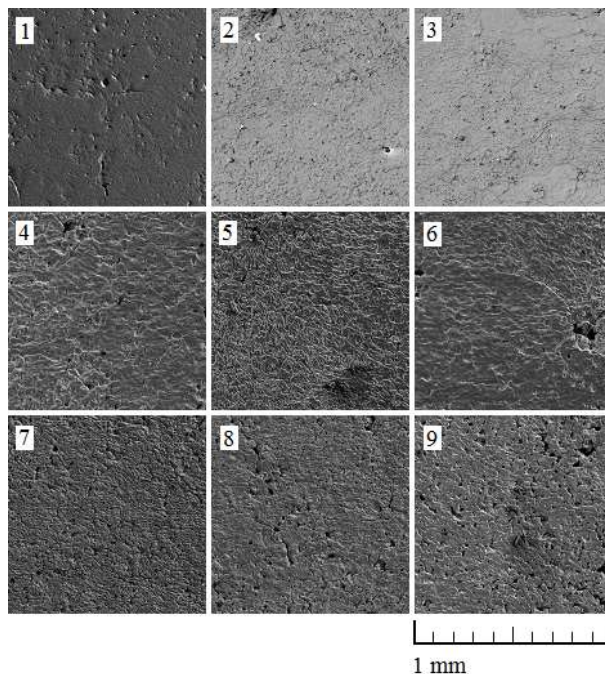

Figure 9
Microstructure in specific areas No. 1–9 of the thin plate surface (×166)

Figure 9 shows the microstructure of one of the thin plates, obtained using the scanning electronic microscope Tescan Vega II XMU. The actual size of areas No. 1–9: height – 1 mm, width – 1 mm. It is obvious that in the horizontal layer of the material, which is in close to the upper punch, the porosity reduces from area 1 towards area 3.

The consistency of porosity distribution pattern in the material lying on the bottom of the container has an inverse dependence, as compaction occurs from area 9 towards area 7.

In the vertical direction, the surface porosity of areas 1–3 is substantially less when compared to areas No. 7–9. The porosity in various areas of the thin plate surfaces was established by the method of quantitative metallography with the application of image processing and analysis with the help of Matlab software. The statistical processing of the experimental data, obtained after the quantitative evaluation of microstructure, was carried out at the confidence level of 0.95. The method of maximal relative deviation computation was used for the verification of the obtained data for normality of distribution and elimination of gross errors.
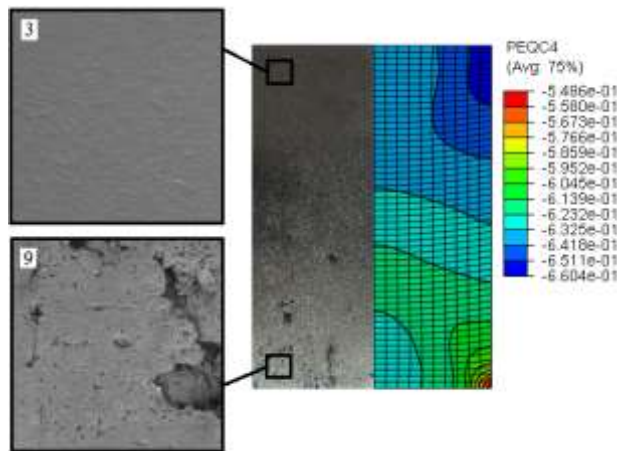

Figure 10

Distribution of total volumetric inelastic strain in the workpiece cross section (right) and microstructure of the thin plate surface (left)

Figure 10 shows the results of the FE simulation die compaction and the microstructure of the work-piece cross-section, obtained by means of electron microscopy. One can see that the distribution of the total volumetric inelastic strain in the work-piece cross-section is in agreement with the material surface porosity distribution on thin plate. The highest value of volume strain is localized in the area adjacent to the upper punch and grows from the center towards periphery; consequently, this area of compacted workpiece will show the lowest porosity value.

In the work-piece center, the level lines of volume strain tend to horizontal position. Coming closer to the edge layers of the work-piece, the horizontal layer compaction is broken. The area of the lowest values of volume strain is located at the junction of the punch and the side surface of the container bottom, here the hydrostatic pressures are less active and their value grows inversely – from the periphery towards the center.

Table 1 shows the comparison of FE simulation and experimental results in specific areas of the briquette cross section.

Table 1

Porosity of the material depending on the tensor stress components (mean stress)
in the areas No. 1–9 after die compaction

	Area No.								
	1	2	3	4	5	6	7	8	9
q, MPa	576	617	794	519	539	564	494	444	257
p, MPa	384	413	526	347	356	368	324	290	171
σ_1, MPa	-192	-207	-255	-173	-175	-179	-158	-139	-88
σ_2, MPa	-768	-824	-1054	-692	-709	-732	-653	-585	-342
σ_3, MPa	-192	-207	-255	-173	-175	-179	-158	-139	-88
θ, % (experiment)	1.32	0.82	0.60	1.96	1.73	1.34	2.18	2.84	5.90
θ, % equation (6)	0.80	0.59	0.18	1.18	1.08	0.95	1.50	2.14	7.47

It is obvious that each of the 9 areas (corresponding to the column head numbers of the table) of the work-piece cross-section has unique stress state characteristics. The most effective compaction takes place in area No. 3, where von Mises equivalent stresses value has a maximum value $q = 794$ MPa and the highest equivalent pressure stress occur $p = 526$ MPa. Area No. 9 shows the minimal density, characterized by the lowest value of von Mises equivalent stresses $q = 257$ MPa and by the value of $p = 171$ MPa.

Conclusions

On the basis of the FE simulation of multiaxial compression process of titanium sponge, the dependence of porosity variation on the value of equivalent pressure stress and von Mises equivalent stresses has been established. It was found that equivalent pressure stress produces a more substantial effect on compaction of material as compared to the effect of shear stress. Nevertheless, in case of a stress condition corresponding to the scheme of isostatic compression, the obtained powdered material porosity has not been less than 6%. It has been shown, that production of quasimonolythic material with a minimal porosity value is only possible at joint action of normal and shear deformations. In order to verify the results of FE simulation, the experiments on compaction of titanium sponge in a closed die were carried out. It was shown that the consistency pattern of the material porosity distribution corresponds to the regularity of changing the field of equivalent pressure stress and the value of von Mises equivalent stresses, obtained by the way of FE analysis.

References

[1]   N. A. Shestakov, V. N. Subich, V. A. Demin: Uplotnenie, konsolidatsiya i razrushenie poristykh materialov (in Russian), Moscow, FIZMALIT, 2009

[2]   K. L. Nielsen, J. Dahl, V. Tvergaard: Collapse and Coalescence of Spherical Voids Subject to Intense Shearing: Studied in Full 3D. International Journal of Fracture, Vol. 177, Iss. 2, pp. 97-108, 2012

[3]   V. Tvergaard: Behaviour of Voids in a Shear Field. International Journal of Fracture, Vol. 158, Iss. 1, pp. 41-49, 2009

[4]   G. A. Baglyuk, A. I. Khomenko: Osobennosti deformirovannogo sostoyaniya poristykh zagotovok pri ikh zakrytoi i otkrytoi shtampovke. (in Russsian) Izvestiya vuzov. Tsvetnaya metallurgiya, No. 1, pp. 57-62, 2015

[5]   S. C. Lee, K. T. Kim: Densification Behavior of Aluminium Alloy Powder under Cold Compaction. International Journal of Mechanical Sciences, Vol. 44, Iss. 7, pp. 1295-1308, 2002

[6]   H. Shin, J. B. Kim, S. J. Kim, K. Y. Rhee: A Simulation-based Determination of Cap Parameters of the Modified Drucker–Prager Cap Model by Considering Specimen Barreling during Conventional Triaxial Testing. Computational Materials Science, Vol. 100, Part A, pp. 31-38, 2015

[7]   P. Doremus, C. Geindreau, A. Martin, L. Debove, R. Lecot: High Pressure Triaxial Cell for Metal Powder. Powder Metallurgy, Vol. 38, Iss. 4, pp. 284-287, 1995

[8]   A. D. Hartman, S. J. Gerdemann, J. S. Hansen: Producing Lower-Cost Titanium for Automotive Applications. The Journal of The Minerals, Metals & Materials Society, Vol. 50, No. 9, pp. 16-19, 1998

[9]   M. P. Bondar, B. V. Voitsekhovskii, E. S. Obodovskii, V. A. Kharchenko: O svoistvakh kompaktnogo titana, poluchennogo obrabotkoi davleniem gubchatogo titana. (in Russia) Tsvetnye metally, Vol. 12, pp. 75-78, 1978

[10] A. M. Laptev, E. S. Obodovskii: Plastic Deformation of Sponge Titanium. Powder Metallurgy and Metal Ceramics, Vol. 25, Iss. 7, pp. 547-552, 1986

[11] E. S. Obodovskii, A. M. Laptev: Effect of Technological Factors on the Properties of High-Density Titanium Sponge Compacts. Powder Metallurgy and Metal Ceramics, Vol. 26, Iss. 4, pp. 295-299, 1987

[12] A. G. Zalazinskii, V. I. Novozhonov, V. L. Kolmykov, M. V. Sokolov: Modelirovanie pressovaniya briketov i vydavlivaniya prutkov iz titanovoi gubki.(I Russia) Metally, No. 6, pp. 64-68, 1997

[13] I. Sh. Trakhtenberg, A. B. Borisov, V. I. Novozhonov, A. P. Rubshtein, A. B. Vladimirov, A. V. Osipenko, V. A. Mukhachev, E. B. Makarova: Mechanical Properties and the Structure of Porous Titanium Obtained by

Sintering Compacted Titanium Sponge. The Physics of Metals and Metallography. Vol. 105, No. 1, pp. 92-97, 2008

[14]   A. Hadadzadeha, M. A. Whitney, M. A. Wells, S. F. Corbin: Analysis of Compressibility Behavior and Development of a Plastic Yield Model for Uniaxial Die Compaction of Sponge Titanium Powder. Journal of Materials Processing Technology. Vol. 243, pp. 92-99, 2017

[15]   WO 2011049465 A1. Method for Production of Titanium Welding Wire

[16]   WO 2012127426 A1. Method for Production of Alloyed Titanium Welding wire

[17]   A. V. Nesterenko, V. I. Novozhonov, A. G. Zalazinskii, A. V. Skripov: Influence of Temperature on Compactibility of Briquettes of Titanium Sponge Alloyed with Hydrogen. Russian Journal of Non-Ferrous Metals, Vol. 56, No. 3, pp. 287-292, 2015

[18]   I. Berezin, A. Nesterenko, A. Zalazinsky, N. Michurov: "Finite-Element Simulation of Multiaxial Compaction of Sponge Titanium Powder" in Mechanics, Resource and Diagnostics of Materials and Structures (MRDMS–2016) 1785, AIP Conference Proceedings, edited by E. Gorkunov et al. (American Institute of Physics, Melville, NY, 2016), pp. 040008-1-040008-4

[19]   ABAQUS 6.10 Theory Manual, Dassault Systemes Simulia Corp., Providence, RI, USA, 2010

[20]   L. H. Han, J. A. Elliott, A. C. Bentham, A. Mills, G. E. Amidon, B. C. Hancock: A Modified Drucker–Prager Cap Model for Die Compaction Simulation of Pharmaceutical Powders. International Journal of Solids Structures, Vol. 45, Iss. 10, pp. 3088-3106, 2008

[21]   B. S. Zhang, M. Jain, C. H. Zhao, M. Bruhis, R. Lawcock, K. Ly: Experimental Calibration of Density-Dependent Modified Drucker–Prager Cap Model using an Instrumented Cubic Die for Powder Compact. Powder Technology, Vol. 204, Iss. 1, pp. 27-41, 2010

[22]   C. Shang, I. C. Sinka, J. Pan: Constitutive Model Calibration for Powder Compaction Using Instrumented Die Testing. Experimental Mechanics, Vol. 52, Iss. 7, pp. 903-916, 2012

[23]   S. Garner, J. Strong, A. Zavaliangos: The Extrapolation of the Drucker–Prager/Cap Material Parameters to Low and High Relative Densities. Powder Technology, Vol. 283, pp. 210-226, 2015

[24]   C. Pavanachand, R. Krishnakumar: Yield Function Parameters for Metal Powder Compaction based on Unit Cell Studies. Acta Materialia, Vol. 45, Iss. 4, pp. 1425-1444, 1997

[25]   V. E. Panin, V. A. Likhachev, Yu. V. Grinyaev: Strukturnye urovni deformatsii tverdykh tel. (in Russia) Novosibirsk: Nauka, 1985

[26]   R. J. Henderson, H. W. Chandler, A. R. Akisanya, C. M. Chandler, S. A. Nixon: Micro-Mechanical Modelling of Powder Compaction. Journal of the Mechanics and Physics of Solids, Vol. 49, Iss. 4, pp. 739-759, 2001

[27]   N. Ogbonna, N. A. Fleck: Compaction of an Array of Spherical Particles. Acta Metallurgica et Materialia, Vol. 42, Iss. 2, pp. 603-620, 1995

[28]   A. Benabbes, L. Dormieux, L. Siad: An Estimate of the Macroscopic Yield Surfaces of Powder Compacts using the Kinematic Approach of the Yield Design Theory. International Journal of Material Forming, Vol. 1, pp. 53-56, 2008

[29]   XJ. Xin, P. Jayaraman, G. S. Daehn, R. H. Wagoner: Investigation of Yield Surface of Monolithic and Composite Powders by Explicit Finite Element Simulation. International Journal of Mechanical Sciences, Vol. 45, Iss. 4, pp. 707-723, 2003

[30]   S. J. Subramanian, P. Sofronis: Calculation of a Constitutive Potential for Isostatic Powder Compaction. International Journal of Mechanical Sciences, Vol. 44, Iss. 11, pp. 2239-2262, 2002

[31]   H. Li, S. Saigal, P. T. Wang: A Solution for the Contact between Two Spherical Particles Undergoing Large Deformation. Acta Materialia, Vol. 44, Iss. 7, pp. 2591-2598, 1996

[32]   C. Tsigginos, J. Strong, A. Zavaliangos: On the Force-Displacement Law of Contacts between Spheres Pressed to High Relative Densities. International Journal of Solids and Structures, Vol. 60-61, pp. 17-27, 2015

[33]   Yu. A. Aksenov, I. O. Bashkin, V. L. Kolmogorov, E. G. Ponyatovskii, G. G. Taluts, V. K. Kataya, I. V. Levin, Yu. I. Potapenko, A. N. Trubin: Vliyanie vodoroda na plastichnost' i soprotivlenie deformatsii tekhnicheskogo titana VT1-0 pri temperaturakh do 750 °C. FMM, Vol. 67, No. 5, pp. 993-999, 1989